

## Creating atomic Stokes vortices with spin-1 atomic wave functions

Maitreyi Jayaseelan <sup>1,2,\*</sup>, Joseph D. Murphree <sup>1,2</sup>, Justin T. Schultz <sup>2,3</sup> and Nicholas P. Bigelow <sup>1,2,3</sup>

<sup>1</sup>*Department of Physics and Astronomy, University of Rochester, Rochester, New York 14627, USA*

<sup>2</sup>*Center for Coherence and Quantum Optics, University of Rochester, Rochester, New York 14627, USA*

<sup>3</sup>*The Institute of Optics, University of Rochester, Rochester, New York 14627, USA*



(Received 22 January 2023; revised 3 July 2023; accepted 18 August 2023; published 14 September 2023)

The formal correspondences between pseudo-spin-1/2 systems in optics and in atomic physics have provided fertile ground for exploring polarization in atom optics. Previous experimental results demonstrated atomic polarimetry techniques for two-level wave functions and explored wave-field singularities in the multicomponent wave function of a spinor Bose-Einstein condensate using visualization techniques developed in optics [J. T. Schultz, A. Hansen, and N. P. Bigelow, *Opt. Lett.* **39**, 4271 (2014); A. Hansen, J. T. Schultz, and N. P. Bigelow, *Optica* **3**, 355 (2016)]. Here we further this discussion, reexamining the atomic Stokes parameters and Stokes polarimetry in the context of spin-1 systems where the tensor moments of the higher-spin system enrich the physics considerably. We show that our atomic polarimetry methods provide tools to engineer the multipole tensor moments of the higher-spin atomic wave function, and to realize nontrivial couplings between these multipole moments and an atomic center-of-mass orbital angular momentum. The different forms of coupling between internal tensor moments and external angular momenta can be used to realize a variety of topological structures in the atomic wave field. We identify these  $\pi$ - and  $2\pi$ -symmetric features in the streamlines of the atomic Stokes fields constructed in analogy with singular optics.

DOI: [10.1103/PhysRevA.108.033311](https://doi.org/10.1103/PhysRevA.108.033311)

### I. INTRODUCTION

Atom optics connects the fields of optics and atomic physics. Atomic analogs of many optical elements, including lenses, beamsplitters, and interferometers, have already been developed for applications in precision interferometry, sensing, and metrology [1]. The availability of internal degrees of freedom in atomic systems allows us to explore polarization in atom optics.

In previous work from our group, we investigated atom-optic polarization using a correspondence between two pseudo-spin-1/2 systems: the circular polarization states of a transverse optical field, and the energy eigenstates of a two-level atom. In the pseudo-spin-1/2 framework, we defined the atomic Stokes parameters that characterize an arbitrary atomic state, and developed atomic analogs of optical waveplates with a coherent two-photon Raman interaction. Using these results, we demonstrated a form of atomic Stokes polarimetry to extract the Stokes parameters of an atomic wave function [2]. Our techniques have allowed us to explore the rich physics of wave-field singularities in atomic systems. By drawing on foundations of singular optics, we realized atomic counterparts to vector-vortex beam fields, full-Poincaré beams, optical  $q$ -plates, and more [3,4].

The availability of higher-spin manifolds and external degrees of freedom in these systems enriches the physical landscape considerably. High-spin systems (spin  $> 1/2$ ) must be characterized not only by their rank-1 spin moments, but also by their higher-order tensor moments: a spin-1 system

for instance must be described by both its “orientation,” captured by the first-order (vector) moments of the spin operators, and its “alignment,” captured by the second-order (quadrupolar) moments. The alignment is typically described with a  $\pi$ -symmetric nematic director which defines the long axis of broken symmetry for a system with quadrupolar order. Such nematic directors are seen in many physical systems, with a well-known example being the long rodlike molecules of nematic liquid crystals: the head-to-tail symmetry of the molecules’ long axis allows their orientational order to be described by a headless nematic director.

In optics, the higher-order tensor wave fields associated with light have been extensively studied in the context of polarization, where the invariance of the polarization ellipse under a  $\pi$  rotation is a signature of the second-order tensor moment of the optical field. Phase and polarization singularities in these wave fields display a variety of interesting features, including  $\pi$ - and  $2\pi$ -symmetric structures in field streamlines [5], fractionally quantized photon total angular momenta [6,7], Möbius bands [8], and knots [7]. Many of these features are brought about by a coupling between the intrinsic and extrinsic momenta of the system and play important roles in polarimetry, singular optics, and quantum information.

Here, we move beyond the pseudo-spin-1/2 description to extend the discussion of atom-optic polarization to spin-1 systems, using the multicomponent wave function of an <sup>87</sup>Rb spinor Bose-Einstein condensate. We present a theoretical development of the language of atom optics to include higher-order (rank-2) tensor moments of the atomic wave field and show experimental data to illustrate physical realizations of the phenomena we describe.

\*Corresponding author: [maitreyi.jayaseelan@colorado.edu](mailto:maitreyi.jayaseelan@colorado.edu)

We tailor the spin-1 atomic multipole components using nonlinear light-matter interaction Hamiltonians composed of a combination of rank-2 and rank-1 operators. Within the spin-1 framework, we develop the discussion of the Raman waveplate and atomic Stokes polarimetry to examine the various forms of coupling of internal (spin tensor) and external (orbital) angular momenta in the system. Such couplings have been of both theoretical and experimental interest in atomic physics over the last decade [9–17], and the language of atomic physics offers a powerful machinery that allows us to highlight these couplings explicitly. We show using appropriate gauge transformations that our results [2] on atomic Stokes polarimetry can be cast as experimental realizations of a *spin-nematic* vortex state, and *nematic-orbit* states, when considered within the spin-1 framework. These states feature a coupling between orbital angular momentum (OAM) and the higher-order tensor moments of the wave function: in the spin-nematic state, the coupling of OAM and spin results in a vortex structure appearing in the nematic components of the cloud, while in the nematic-orbit states, the coupling is between OAM and a nematic component of the wave function.

The spin-nematic and nematic-orbit states show fundamentally interesting topological features. We construct atomic Stokes fields for the spin-1 wave function in analogy with similar studies in optics, and identify a variety of wave-field features using language from singular optics. Given the similarities between the atomic and optical systems, we foresee further opportunities to unify the two fields with a common language in order to continue to combine expertise that has been independently developed.

## II. THEORETICAL FRAMEWORK

### A. Spin-1 description of optical polarization

For a paraxial optical field with no component of polarization in the direction of propagation, the electric field may be written as  $\mathbf{E}(t) = \text{Re}[(E_+ \mathbf{e}_+ + E_- \mathbf{e}_-) e^{-i\omega t}]$ , with  $\omega$  the frequency and  $E_+$  and  $E_-$  the right and left circular polarization components of the field. In the spherical basis  $(\mathbf{e}_+, \mathbf{e}_0, \mathbf{e}_-)$ , a statistical description of polarization is then provided by the coherency matrix [18]

$$\Phi_3(\mathbf{E}) = \frac{1}{2} \begin{pmatrix} S_0 + S_3 & 0 & -(S_1 - iS_2) \\ 0 & 0 & 0 \\ -(S_1 + iS_2) & 0 & S_0 - S_3 \end{pmatrix}, \quad (1)$$

where  $S_i$  are the optical Stokes parameters [19]. Since the full symmetry group for spin-1 is the group  $\text{su}(3)$ , there are eight independent operators, including three spin operators  $\mathbf{F} = \{\hat{F}_x, \hat{F}_y, \hat{F}_z\}$  and five nematic operators that are quadratic forms composed of the spin operators, that provide a basis for the system. By examining the components of the coherency matrix in this basis, we find that in paraxial optics, only a subset of these operators plays a role: the Stokes parameters  $S_1, S_2,$  and  $S_3$  that characterize paraxial fields are obtained as the expectation values of the operators  $\mathbf{Q} \equiv \{\hat{Q}_{x^2-y^2}, \hat{Q}_{xy}, \hat{F}_z\}$  for the field, where  $\hat{Q}_{x^2-y^2} = \hat{F}_x \hat{F}_x - \hat{F}_y \hat{F}_y$  and  $\hat{Q}_{xy} = \hat{F}_x \hat{F}_y + \hat{F}_y \hat{F}_x$ .

We note that the operators  $\mathbf{Q}$  form an  $\text{su}(2)$  subalgebra of  $\text{su}(3)$ , so that the system may be treated within the familiar

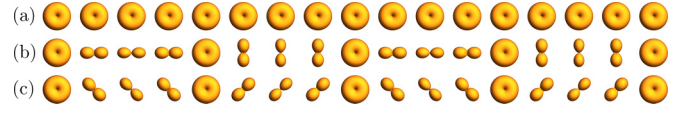


FIG. 1. Spherical harmonic representations showing the transformations effected by a unitary operator of the form  $e^{i\varphi\hat{Q}_i}$  on the wave function  $|\psi_0\rangle = (1, 0, 0)^T$ , shown at intervals of  $\varphi = \pi/8$  and with  $\hat{Q}_i$  the operators (a)  $\hat{F}_z$ , (b)  $\hat{Q}_{xy}$ , and (c)  $\hat{Q}_{x^2-y^2}$ . Shown are the surface plots of  $|\psi(\hat{s})|^2$  representing the magnitude of the wave function in spin space, where  $\psi(\hat{s})$  is the spin space representation [Eq. (2)] of the wave function  $|\psi\rangle = e^{i\varphi\hat{Q}_i}|\psi_0\rangle$ . Here  $x$  and  $y$  are the horizontal and vertical directions, and  $z$  is out of the page.

pseudo-spin-1/2 formalism. However, the spin-1 description used here allows us to recognize the tensor composition of the field in the symmetries of the polarization ellipse: linear polarization is symmetric under a rotation by  $\pi$ , and characterizes the rank-2 quadrupolar component of the coherence matrix, while circular polarization is associated with the rank-1 component. A pseudo-spin-1/2 description obscures the tensorial characteristics of the system.

### B. Spin-1 description of atomic wave functions

We may now construct a more complete atom-optic analog of transverse optical polarization in spin-1 atomic systems. Since the Stokes parameters are the expectation values of the operators  $\mathbf{Q}$ , we must develop tools to engineer and characterize these multipolar components of an atomic wave function.

To this end, in Fig. 1 we show how the operators  $\mathbf{Q}$  transform the atomic wave function  $|\psi_0\rangle = (1, 0, 0)^T$ , which is initially oriented along  $\hat{F}_z$  and is the atomic analog of a state of circular polarization. The spherical harmonics show the surface plot of the wave function  $|\psi(\hat{s})|^2$  where  $|\psi(\hat{s})\rangle$  is the decomposition of the spin-1 wave function  $|\psi\rangle$  into its spherical harmonic components  $Y_{1,m}(\hat{s})$ ,

$$|\psi(\hat{s})\rangle = \sum_{m=-1}^1 \psi_m Y_{1,m}(\hat{s}), \quad (2)$$

and  $\hat{s}$  is a unit vector in spin space depicting the local spin orientation [20].

We make two observations from Fig. 1.

(1) The symmetry of the wave function can be changed by transformations generated by  $\hat{Q}_{x^2-y^2}$  and  $\hat{Q}_{xy}$ , which are quadratic forms of the spin operators. That is, the wave function develops rank-2 ( $\pi$ -symmetric) components in Figs. 1(b) and 1(c), analogous to linear polarization in optics. This is in contrast to transformations generated by spin operators themselves, which merely produce rotations of a state in spin space but do not change their symmetry.

(2) The wave function does not develop any other rank-1 or rank-2 components, other than components in  $\mathbf{Q}$ . This is because the operators  $\mathbf{Q}$  form an  $\text{su}(2)$  subalgebra of  $\text{su}(3)$ ; the Baker-Campbell-Hausdorff lemma [21] then helps to verify that an atomic wave function with components restricted to these specific basis states will continue to be so restricted under transformations generated by these operators.

Again, we note that since the operators  $\mathbf{Q}$  form an  $\text{su}(2)$  subalgebra of  $\text{su}(3)$ , the system may be considered in the pseudo-spin-1/2 framework, where the transformations are

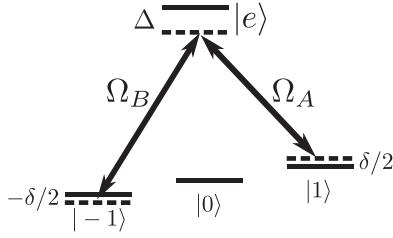


FIG. 2. Raman coupling in a spin-1 system.

generated by the Pauli matrices. However, the  $\pi$  symmetry of the wave function and the sculpting of multipole moments with quadratic forms of the spin operators cannot be described in this reduced space, since quadratic forms of the Pauli operators are proportional to the identity. Thus, in order to control the tensor moments of a spin-1 atomic wave function in analogy with paraxial optics and to generate an interconversion of spin orientation and alignment, we must realize nonlinear interaction Hamiltonians composed of a combination of the spin and nematic operators  $\mathbf{Q}$ .

### III. RAMAN COUPLING IN SPIN-1

#### A. Hamiltonian engineering of the spin-1 wave function

We now turn to a theoretical description of the experimental system. Our system is composed of three ground atomic energy eigenstates labeled  $\{|1\rangle, |0\rangle, |-1\rangle\}$ . We employ a coherent two-photon Raman process to couple the two ground states  $|1\rangle$  and  $|-1\rangle$  via an excited state  $|e\rangle$ , using optical fields with Rabi frequencies  $\Omega_A$  and  $\Omega_B$  and  $(\sigma_-, \sigma_+)$  polarizations (Fig. 2). For large single-photon detuning,  $\Delta$ , of the lasers from  $|e\rangle$ , the excited state can be adiabatically eliminated and the three ground-state levels constitute a spin-1 system.

To simplify our treatment, we use  $|\Omega_A| = |\Omega_B| = |\Omega|$ . The effective Rabi frequency between the two coupled ground states is  $\Omega_R(r) = |\Omega(r)|^2/4\Delta$ , where  $r$  is the radial coordinate. Denoting the relative phase between the Raman beams as  $\beta$ , the total laboratory frame Hamiltonian, including the kinetic-energy term and the Raman interaction, has a general form given by

$$\mathcal{H}_{\text{lab}}(\beta, \delta) = -\frac{1}{2}\nabla^2 - \Omega_R(r)\hat{F}_z^2 - \mathbf{\Omega}_{\text{eff}} \cdot \mathbf{Q}. \quad (3)$$

The effective light-induced coupling term of the Hamiltonian is through  $\mathbf{\Omega}_{\text{eff}} \cdot \mathbf{Q}$  with  $\mathbf{\Omega}_{\text{eff}} \equiv (\Omega_R(r)\cos\beta, \Omega_R(r)\sin\beta, -\delta/2)$ , where  $\delta$  is the two-photon detuning. The parameters  $\beta$ ,  $\delta$ , and  $\Omega_R(r)$  and the time of the Raman interaction  $\tau$  are experimentally controlled. Note that the relative phase between the Raman beams ( $\beta$ ) and the effective Rabi frequency  $[\Omega_R(r)]$  may be spatially varying. The Raman Hamiltonian thus provides a versatile tool to engineer the atomic wave function, allowing control of its tensor components  $\langle \mathbf{Q} \rangle$ .

#### B. Raman waveplate Hamiltonians in spin-1

A special case of the Raman Hamiltonian is obtained for two-photon detuning  $\delta = 0$  and spatially uniform Rabi frequencies and relative phase  $\beta$ , and for square diabatic pulses. In this special case, the interaction portion of Eq. (3) is the atomic analog of an optical waveplate: the effect of this

Raman waveplate on a pseudo-spin-1/2 atomic wave function is analogous to the effect of an optical waveplate on an electric field [2]. We give a brief description of the Raman interaction in the pseudo-spin-1/2 regime in Appendix A, and the Raman waveplate and atomic Stokes polarimetry in the pseudo-spin-1/2 regime in Appendix B.

We may examine the Raman waveplate Hamiltonian in the spin-1 context, noting that the pseudo-spin-1/2 case is recovered by neglecting the basis state  $|0\rangle$ . For Raman beams with spatially uniform relative phase  $\beta$  and Rabi frequency  $\Omega_R$  the Raman interaction portion of the Hamiltonian of Eq. (3) is

$$\mathcal{H}_{\text{WP}}(\beta) \equiv \mathcal{H}_{\text{lab}}(\beta, \delta = 0) \\ = -\Omega_R(\hat{F}_z^2 + \cos\beta\hat{Q}_{x^2-y^2} + \sin\beta\hat{Q}_{xy}). \quad (4)$$

Comparing this with the Raman waveplate for pseudo-spin-1/2 systems [2], we recognize that this is an effective waveplate Hamiltonian in the transverse subspace with waveplate angle  $\beta/2$ , and retardance determined by total pulse area  $\Omega_R\tau$  for interaction time  $\tau$ . Quarter and half waveplates at arbitrary angles  $\beta/2$  are realized by tuning the interaction time such that  $\Omega_R\tau = \pi/4$  or  $\pi/2$ .

In optics, waveplates perform interconversions of linear and circular polarization states of light. In the spin-1 atomic system, the Raman waveplate of Eq. (4) performs analogous transformations, interconverting the rank-2 and rank-1 moments of the wave function. The mechanism for the interconversion of these atomic tensor moments is highlighted by considering particular waveplate Hamiltonians: for  $\beta = 0, \pi/2, \pi$ , and  $3\pi/2$ , we find that Eq. (4) has the same form as nonlinear twisting Hamiltonians,<sup>1</sup> specifically,

$$\begin{aligned} \mathcal{H}_{\text{WP}}(\beta = 0) &= -\Omega_R(\hat{F}_z^2 + \hat{Q}_{x^2-y^2}) \\ &= -\Omega_R(\hat{F}^2 - 2\hat{F}_y^2), \\ \mathcal{H}_{\text{WP}}(\beta = \pi/2) &= -\Omega_R(\hat{F}_z^2 + \hat{Q}_{xy}) \\ &= -\Omega_R(\hat{F}^2 - (\hat{F}_x - \hat{F}_y)^2), \\ \mathcal{H}_{\text{WP}}(\beta = \pi) &= -\Omega_R(\hat{F}_z^2 - \hat{Q}_{x^2-y^2}) \\ &= -\Omega_R(\hat{F}^2 - 2\hat{F}_x^2), \\ \mathcal{H}_{\text{WP}}(\beta = 3\pi/2) &= -\Omega_R(\hat{F}_z^2 - \hat{Q}_{xy}) \\ &= -\Omega_R(\hat{F}^2 - (\hat{F}_x + \hat{F}_y)^2). \end{aligned} \quad (5)$$

These expressions offer an intuitive way to understand the interconversion of spin orientation and alignment of our wave function, and will allow a straightforward treatment of our atomic polarimetry techniques.

#### C. Atomic Stokes polarimetry in spin-1

With the spin-1 description of the Raman waveplate in place, we can now describe our atomic polarimetry techniques in the spin-1 context. We demonstrate this technique on a wave function of the form

$$|\psi\rangle = \psi_1|1\rangle + e^{i\phi}\psi_{-1}|-1\rangle, \quad (6)$$

<sup>1</sup>Hamiltonians with these forms are important in the context of spin squeezing, and give rise to modifications in the structure of fluctuations in multispin systems [22].

where  $\phi$  denotes the azimuthal coordinate, so that  $e^{i\phi}$  is an azimuthal phase term.

We create a wave function of this form using a Raman pulse pair with Gaussian (G) and Laguerre-Gaussian (LG) beam profiles. The relative azimuthal phase of these Raman beams,  $\beta = \phi$ , is imprinted onto the wave function as the relative phase between the spin states. Further experimental details are given in Appendix C.

Stokes polarimetry is performed in analogy with optical Stokes polarimetry, by obtaining spin state population measurements of  $|\psi\rangle$  in three orthogonal bases. Our Stokes polarimetry measurements rely on a Stern-Gerlach absorption imaging process that yields spatially resolved spin state information in the  $\hat{F}_z$  basis. A direct measurement of the wave function thus yields  $|\psi_1|^2$  and  $|\psi_{-1}|^2$ . The parameter  $S_3 \equiv \langle \hat{F}_z \rangle = |\psi_1|^2 - |\psi_{-1}|^2$  is then obtained by subtracting these two measurement results [Fig. 3(c)]. The sum of the two measurements gives  $S_0$ , the total population. Measurements of  $S_1 \equiv \langle \hat{Q}_{x^2-y^2} \rangle$  and  $S_2 \equiv \langle \hat{Q}_{xy} \rangle$  are obtained by using Raman quarter waveplates with  $\beta = \pi/2$  and 0 to perform a rotation of the measurement basis prior to Stern-Gerlach imaging [Figs. 3(a) and 3(b)]. The measurement results in the rotated bases are then subtracted to give  $S_1$  and  $S_2$ . This is in analogy with optics, where waveplates transform the polarization of light between circular and linear bases prior to measurement with a beamsplitter.

In Fig. 3, we show the results of atomic Stokes polarimetric measurements of  $|\psi\rangle$ , with corresponding theory maps. The experimental data in the first two columns in each set of images are averages of two-to-three single-shot absorption images of spatially separated spin components of a Bose-Einstein condensate. Inhomogeneities in the spatial modes of the Raman beams, inhomogeneities in the shape of the atomic cloud, and noise particularly in regions of low atomic density contribute to experimental noise in the images. Further, the Stokes parameters that we measure are reconstructed from the cloud column densities, and variations of spin state along the long axis of the cloud are integrated out during imaging. Thus, misalignments of the imaging beam—which propagates along the long axis of the atomic cloud—could also contribute to experimental inhomogeneities. The theory maps are fits to the experimental data that use the analytic forms for the wave function after the Raman interaction. Further details are given in Appendix D.

#### IV. COUPLING OF MOMENTA IN STOKES POLARIMETRY

The relative azimuthal phase between the spin components of  $|\psi\rangle$  [Eq. (6)] signifies an extrinsic OAM in the system. Here we show that our atomic polarimetry sequences generate forms of coupling between internal spin tensor momenta and the external orbital angular momentum of the wave function, that are only apparent when the full spin-1 system is considered. In order to identify and analyze these couplings we now turn to the forms of the Hamiltonians used to create  $|\psi\rangle$  and to measure its Stokes parameters.

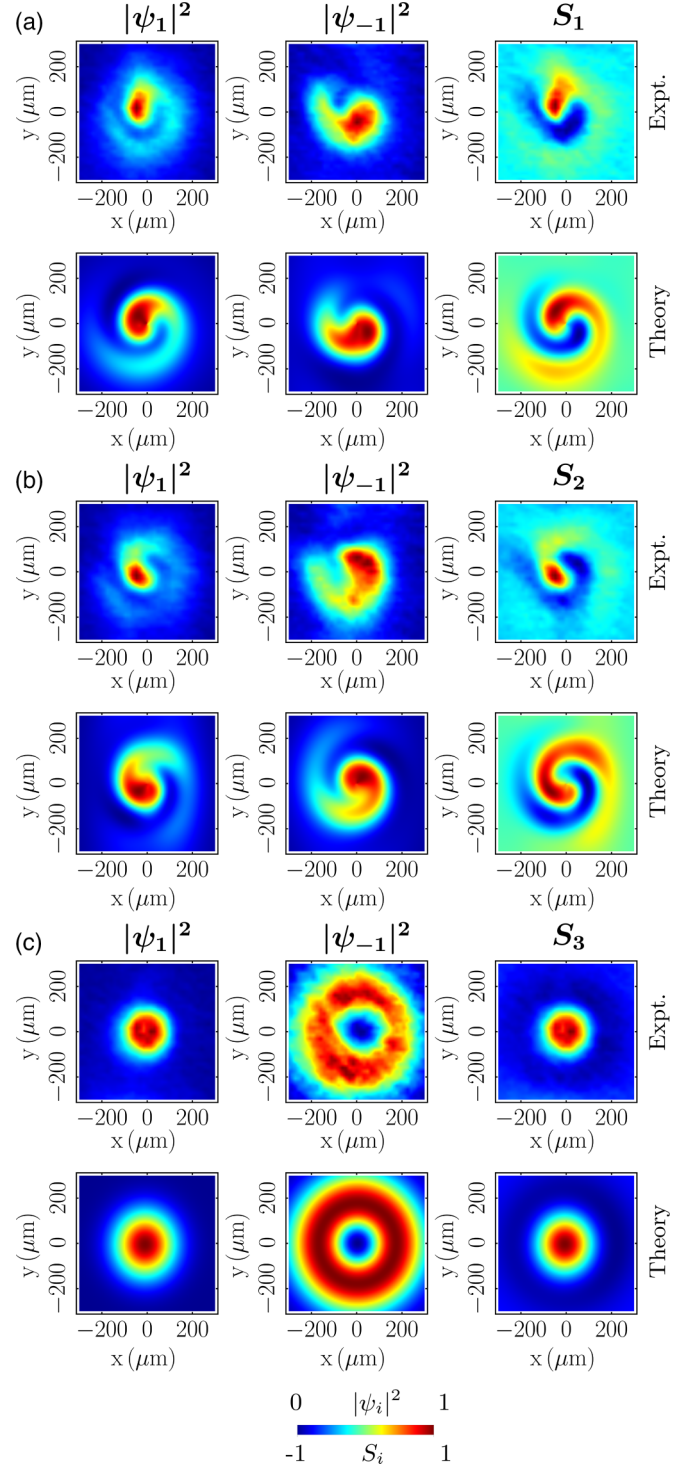


FIG. 3. (a), (b), (c) Experiment (top row) and theory (bottom row) maps showing Stokes parameters  $S_1$ ,  $S_2$ , and  $S_3$  for the wave function  $|\psi\rangle$  of Eq. (6). The first two columns in each panel show spatial maps of the individual spin state populations, with color indicating local atomic density, and normalized within each image. The two measured spin state populations are subtracted to obtain the Stokes parameters shown in the third column of each panel. The length scale is indicated in  $\mu\text{m}$ . Here  $x$  and  $y$  are the horizontal and vertical directions, and  $z$  is out of the page.

### A. Spin-nematic vortex states

As described above,  $|\psi\rangle$  is created using a Raman pulse pair with Gaussian and Laguerre-Gaussian beam profiles. The associated Hamiltonian is obtained by setting the relative phase between the Raman beams to be the azimuthal phase  $\beta = \phi$  so that  $\mathbf{\Omega}_{\text{eff}} = (\Omega_R(r) \cos \phi, \Omega_R(r) \sin \phi, -\delta/2)$  in the Raman interaction Hamiltonian of Eq. (3). For this discussion, we consider the case of two-photon resonance ( $\delta = 0$ ).

There are two points of interest when we examine this Hamiltonian,  $\mathcal{H}_{\text{lab}}(\beta = \phi)$ . First, the vortex structure associated with the azimuthal phase appears in the transverse components of  $\mathbf{Q}$ , that is, in the components associated with spin alignment:  $\hat{Q}_{x^2-y^2}$  and  $\hat{Q}_{xy}$ . This shows that  $|\psi\rangle$  is a spin-nematic vortex state, featuring vorticity in a higher-order tensor moment of the wave function. We will describe the implications of this in the topological features that appear in the associated wave field in Sec. V.

Second, the Hamiltonian couples a well-defined OAM state to a state of definite atomic spin. This coupling is more clearly visible in a gauge that transforms with the nematic components as they change with  $\phi$ , the azimuthal coordinate. The gauge transformation with  $\mathcal{U}_{\text{SN}} = e^{i(\phi/2)\hat{F}_z}$  transforms the Hamiltonian into a frame where the  $\phi$  dependence vanishes.<sup>2</sup> The dressed Hamiltonian (we use a tilde to denote the Hamiltonian after the spatially dependent gauge transformation) is then  $\tilde{\mathcal{H}}_{\text{SN}} = \mathcal{U}_{\text{SN}}\mathcal{H}_{\text{lab}}(\beta = \phi)\mathcal{U}_{\text{SN}}^\dagger$ :

$$\begin{aligned} \tilde{\mathcal{H}}_{\text{SN}} = & -\frac{1}{2}\nabla_{\perp}^2 + \frac{1}{2r^2}\frac{\hat{F}_z^2}{4} - \frac{1}{2r^2}\frac{L_z\hat{F}_z}{2} \\ & - \Omega_R(r)\hat{F}_z^2 - \Omega_R(r)\hat{Q}_{x^2-y^2}. \end{aligned} \quad (7)$$

The coupling between OAM and spin is apparent in the term proportional to  $L_z\hat{F}_z$  where  $L_z = -i\partial_{\phi}$  is the atomic quasi-OAM that is conserved in this frame:  $[L_z, \tilde{\mathcal{H}}_{\text{SN}}] = 0$ .

### B. Nematic-orbit coupled states

Next we examine the Hamiltonians that create the wave functions yielding measurements of  $S_1$  and  $S_2$  for  $|\psi\rangle$ . These Hamiltonians are obtained by transforming  $\mathcal{H}_{\text{lab}}(\beta = \phi)$  with Raman quarter waveplates, using the waveplate Hamiltonians  $\mathcal{H}_{\text{WP}}(\beta = \pi/2)$  and  $\mathcal{H}_{\text{WP}}(\beta = 0)$  [Eq. (5)], and setting  $\Omega_R\tau = \pi/4$ . Transforming with the waveplate  $\mathcal{H}_{\text{WP}}(\beta = \pi/2)$ , the transformed laboratory frame Hamiltonian is  $H_{\text{lab}} = U\mathcal{H}_{\text{lab}}(\beta = \phi)U^\dagger$ :

$$\begin{aligned} H_{\text{lab}} = & -\frac{1}{2}\nabla^2 + U(-\Omega_R(r)\hat{F}_z^2 \\ & - \Omega_R(r)[\cos \phi \hat{Q}_{x^2-y^2} + \sin \phi \hat{Q}_{xy}])U^\dagger \end{aligned} \quad (8)$$

with  $U = \exp[-i\frac{\pi}{4}(\hat{F}^2 - (\hat{F}_x - \hat{F}_y)^2)]$ .

Interestingly, the waveplate interaction transforms the coupling of OAM and spin of the spin-nematic vortex state to a coupling between OAM and the nematic components of the wave function, realizing nematic-orbit coupled wave

functions.<sup>3</sup> This coupling is more clearly visible after a gauge rotation with  $\mathcal{U}_{\text{NO}} = \exp(i\frac{\phi}{2}\hat{Q}_{x^2-y^2})$ , where again the  $\phi$  dependence is removed by the transformation, leaving the quasi-OAM  $L_z$  conserved in this frame. The dressed Hamiltonian (again we use a tilde to denote the Hamiltonian after the spatially dependent gauge transformation)  $\tilde{\mathcal{H}}_{\text{NO}} = \mathcal{U}_{\text{NO}}H_{\text{lab}}\mathcal{U}_{\text{NO}}^\dagger$  is

$$\begin{aligned} \tilde{\mathcal{H}}_{\text{NO}} = & -\frac{1}{2}\nabla_{\perp}^2 + \frac{1}{2r^2}\frac{\hat{F}_z^2}{4} - \frac{1}{2r^2}\frac{L_z\hat{Q}_{x^2-y^2}}{2} \\ & + \Omega_R(r)\hat{F}_z - \Omega_R(r)\hat{F}_z^2. \end{aligned} \quad (9)$$

The coupling between OAM and nematicity is evident in the term proportional to  $L_z\hat{Q}_{x^2-y^2}$ . Similarly, when a quarter waveplate with  $\beta = 0$  is used, the OAM becomes coupled with the operator  $\hat{Q}_{xy}$ .

More generally, acting an arbitrary Raman waveplate on the spin-nematic vortex state realizes a coupling of the form

$$L_z[\sin(\beta)\sin(\gamma)\hat{Q}_{x^2-y^2} - \cos(\beta)\sin(\gamma)\hat{Q}_{xy} + \cos(\gamma)\hat{F}_z] \quad (10)$$

between the OAM and the nematic operator defined by the angles  $(\gamma, \beta)$  where pulse area  $\Omega_R\tau = \gamma/2$ .

## V. TOPOLOGY AND SINGULARITIES WITH ATOMIC STOKES VORTICES

We now examine the singularities and topological features of the wave function  $|\psi\rangle$  [Eq. (6)]. Most simply,  $|\psi\rangle$  hosts a phase singularity in a single spin component, in which the azimuthal phase changes by  $2\pi$  around a singularity where spin state amplitude goes to zero and phase is undefined. However, a discussion of vector (multicomponent) singularities must go beyond a discussion of phase singularities in individual components. In particular for our spin-1 system, the spin-nematic and nematic-orbit coupled states involve the rank-2 moments of the atomic wave function, and thus the topological features of these wave functions must be discussed in the context of a second-order tensor field.

### A. Atomic Stokes fields

Powerful tools with which to study singularities in the second-order tensor field are the complex scalar Stokes fields [23,24]. We define the atomic Stokes fields

$$\Sigma_{ij} \equiv (S_i + iS_j) \quad (11)$$

and the corresponding phase fields

$$\Phi_{ij} = \arg(\Sigma_{ij}). \quad (12)$$

With these definitions, all three Stokes fields for  $|\psi\rangle$  may be constructed from the experimentally measured Stokes parameters (Fig. 3), in analogy with similar studies carried out on an optical lemon field [5].

<sup>2</sup>Note that the structure factor of the  $\text{su}(2)$  subalgebra in consideration here is different than that of the spin matrices: i.e., for the operators  $\mathbf{Q} \equiv \{Q_1, Q_2, Q_3\}$ , we have  $[Q_i, Q_j] = 2i\epsilon_{ijk}Q_k$ , while for the spin operators  $\mathbf{F} \equiv \{F_1, F_2, F_3\}$  we have  $[F_i, F_j] = i\epsilon_{ijk}F_k$ .

<sup>3</sup>Note that Ref. [16] uses the term ‘‘nematic-orbit coupling’’ to refer to a coupling between the linear momentum and nematicity, while we realize a coupling between the orbital angular momentum and nematicity.

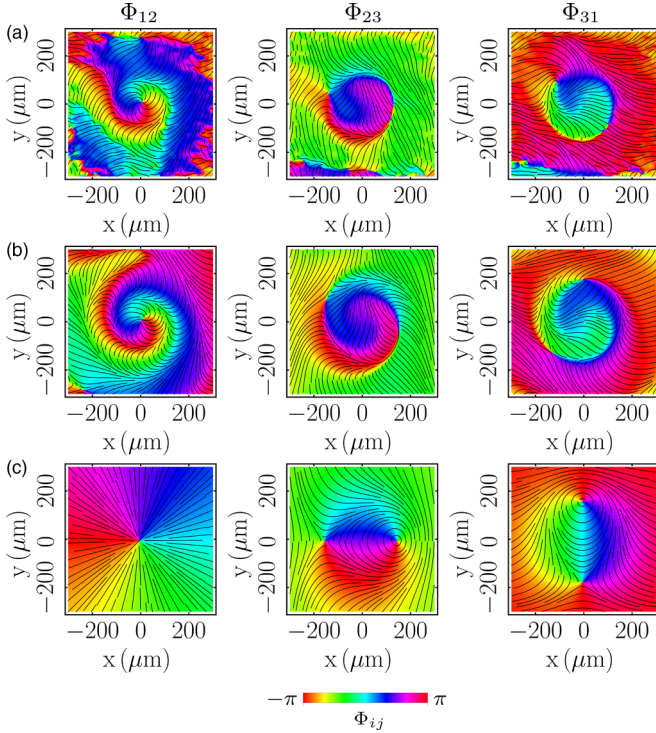


FIG. 4. Stokes phase fields  $\Phi_{ij}$  and streamlines for the wave function  $|\psi\rangle$  of Eq. (6). Here we show (a) experimental data, (b) theory maps taking into account the extra radial phase conferred on the atomic spin states by the spatially varying intensities of the Raman beams, and (c) ideal theory maps where the extra radial phase is absent. The maps show  $2\pi$  symmetric features, with dipole structures appearing in  $\Phi_{23}$  and  $\Phi_{31}$ . The length scale is indicated in  $\mu\text{m}$ . Here  $x$  and  $y$  are the horizontal and vertical directions, and  $z$  is out of the page.

In Fig. 4 we show experimental maps and corresponding theoretical constructions of the atomic Stokes fields associated with  $|\psi\rangle$ . The streamlines indicate the angle of the Stokes phase field: for instance the color light blue, which is the zero phase in the colormap, corresponds to a locally horizontal streamline.

We emphasize that the three Stokes fields are all associated with the same wave function  $|\psi\rangle$ : from the Stokes field definitions we may see that  $\Sigma_{12}$  is converted to  $\Sigma_{23}$  or  $\Sigma_{31}$  using a quarter waveplate oriented at  $\beta/2$ , with  $\beta = \pi/2$  or  $0$ . The atomic polarimetry sequences that deploy Raman quarter waveplates thus provide access to all three Stokes fields for the wave function  $|\psi\rangle$ .

### B. Stokes singularities in the spin-nematic state

The phase field for the Stokes field  $\Sigma_{12} \equiv (S_1 + iS_2)$  is shown in the first column of Fig. 4. The phase field  $\Phi_{12} \equiv \arg(\Sigma_{12})$  gives the relative phase between  $S_1$  and  $S_2$ , and thus characterizes the quadrupolar alignment of the wave function. For the wave function  $|\psi\rangle$ , we have  $S_1 = |\psi_1||\psi_{-1}|\cos\phi$  and  $S_2 = |\psi_1||\psi_{-1}|\sin\phi$ ; thus  $\Phi_{12}$  gives the relative phase  $\phi$  between the two wave-function components of the spin-nematic state, which is the azimuthal phase. This is consistent with

our observation that the spin-nematic vortex state features vorticity in the quadrupolar components.

The phase singularities of the Stokes fields, or Stokes vortices, correspond to component singularities [25]. This means that at a singularity of  $\Phi_{12}$ , either  $|\psi_1|$  or  $|\psi_{-1}|$  must be zero. This is reasoned as follows: since  $\Phi_{12}$  is the relative phase between  $S_1$  and  $S_2$ , both  $S_1$  and  $S_2$  vanish at singularities of  $\Phi_{12}$ . Since the Stokes parameters obey  $\sum_i S_i^2 = 1$ , this implies that  $|S_3| = 1$  at the singularity; for instance  $S_3 = +1$  corresponds to  $|\psi_1| = 1$ , and  $|\psi_{-1}|$  must then be zero. Thus  $\Phi_{12}$  singularities are points of indefinite alignment and definite spin: since  $S_1$  and  $S_2$  characterize the preponderance of the eigencomponents of the quadrupolar operators, the quadrupolar alignment is indefinite when these parameters are zero, as at a singularity of  $\Phi_{12}$ . However, the spin ( $\hat{F}_z$  eigencomponents) takes a definite value.

Singularities of  $\Phi_{12}$  coincide with the conventional  $C$ -point polarization singularities of optics [26]. The Stokes fields thus provide a description of vector field singularities in terms of singularities of a scalar complex field. In the first column of Fig. 4 corresponding to  $\Phi_{12}$ , we can identify a phase singularity of  $\Phi_{12}$ . Comparing this phase distribution with the density distribution of the spin-nematic state of Fig. 3(c), we see that the component  $|\psi_{-1}|^2$  is zero at this location.

The Stokes vortices are associated with integer valued Stokes indices given by  $\sigma_{ij} = \frac{1}{2\pi} \oint \nabla\Phi_{ij} \cdot d\mathbf{l}$ . The phase singularity seen in  $\Phi_{12}$  can be identified as an integer-indexed singularity, around which the phase changes by  $2\pi$ . The streamlines show a radial structure, most clearly visible in the first column of the theory maps in Fig. 4(c). In the experimental data in Fig. 4(a) the Stokes fields show a radial twist as a result of the spatially varying Rabi frequencies of the G-LG Raman pulse pair used to create the spin-nematic wave function (see Appendix A). The theory maps of Fig. 4(b) take into account and model the extra intensity-dependent radial phase. Nevertheless, these streamline plots show the same features as the ideal theory maps that neglect this radial phase.

### C. Stokes singularities in nematic-orbit states

The Stokes fields  $\Sigma_{23} \equiv (S_2 + iS_3)$  and  $\Sigma_{31} \equiv (S_3 + iS_1)$  are shown in the second and third columns of Fig. 4. Just as  $\Phi_{12}$  characterized the relative phase between the wave-function components of  $|\psi\rangle$ ,  $\Phi_{23}$  and  $\Phi_{31}$  characterize the relative phase between the wave-function components of the two nematic-orbit states.

The phase singularities of  $\Phi_{23}$  and  $\Phi_{31}$  correspond to  $x$  or  $y$  and diagonal or antidiagonal component singularities. At a phase singularity of  $\Phi_{23}$  for instance, we must have  $|S_1| = 1$ . This implies that either the  $x$  or the  $y$  component (that is, one of the eigencomponents of  $\hat{Q}_{x^2-y^2}$ ) must be zero. At a phase singularity of  $\Phi_{31}$ , since we must have  $|S_2| = 1$ , either the diagonal or the antidiagonal component (that is, one of the eigencomponents of  $\hat{Q}_{xy}$ ) must be zero. However, comparing the phase distributions with the density distributions of the nematic-orbit wave functions [Figs. 3(a) and 3(b)] is less instructive: since our measurements of the spin state populations are in the spin basis, and the nematic-orbit states are superpositions of the components of  $|\psi\rangle$ , the component

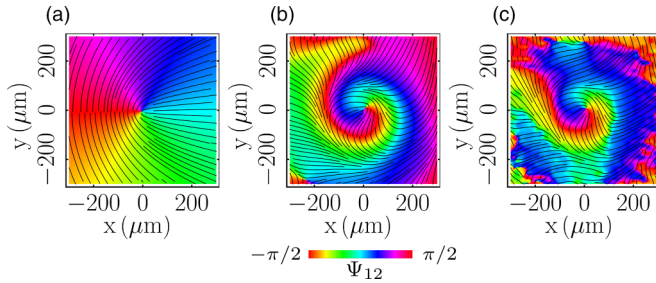


FIG. 5. Half-integer indexed topological structures in the field  $\Psi_{12}$ . Here we show (a) ideal theory structures neglecting the extra radial phase, (b) the theory map taking into account the radial phase, and (c) experimental data (the same data as shown in the first row and column in Fig. 4) here showing the streamlines of  $\Psi_{12}$ . The length scale is indicated in  $\mu\text{m}$ . Here  $x$  and  $y$  are the horizontal and vertical directions, and  $z$  is out of the page.

singularity in these cases does not correspond to a vanishing density in the measured population maps.

The phase fields  $\Phi_{13}$  and  $\Phi_{23}$  show a complex structure with two singular points<sup>4</sup> with opposite phase windings and integer indices  $\pm 1$ . The spatially separated singularities constitute a dipole structure. The size of the dipole depends on the relative amplitudes of the two spin components of  $|\psi\rangle$ . The streamlines of the Stokes fields show saddles and circulation points. These are most clearly visible in the second and third columns of the theory maps in Fig. 4(c). Again, the experimental data shown in Fig. 4(a), and the theory maps of Fig. 4(b) that take into account the extra radial phase, show a twist that distorts the streamlines and the singular structures.

#### D. Half-integer indexed singularities in the atomic wave field

So far, we have discussed the topology of the spin-nematic and nematic-orbit states in terms of the Stokes fields  $\Sigma_{ij}$  and the Stokes indices  $\sigma_{ij}$ . Because the Stokes fields are scalar fields, the vortices of Stokes fields share many of the properties of the more familiar phase vortices in scalar fields [24].

However, the construction of the Stokes fields leads to degeneracies in the types of singularities associated with a particular Stokes index. In optics, for instance, it is well known that the Stokes index cannot distinguish the handedness of polarization  $C$ -point singularities, and it cannot distinguish vector field and ellipse field singularities [27]. These singularities are characterized by Poincaré-Hopf and  $C$ -point indices, which are defined based on the azimuth of the state of polarization of the field [28].

The Stokes index degeneracy prompts us to examine related indices for the atomic wave function. In our system, the relevant index is the  $C$ -point index, which we define in analogy to the optical case through the field  $\Psi_{12} = \Phi_{12}/2$ . This definition takes into account the  $\pi$  symmetry in the orientation of the polarization ellipse or in the quadrupolar

orientation of the spin-1 wave function. The  $C$ -point index is defined in terms of this  $\Psi_{12}$  field as  $I_C = \frac{1}{2\pi} \oint \nabla \Psi_{12} \cdot d\mathbf{l}$ . The Stokes index  $\sigma_{12}$  is thus related to  $I_C$  as  $\sigma_{12} = 2I_C$  [26].

In Fig. 5 we show the phase field  $\Psi_{12}$  associated with the spin-nematic atomic state. We now see the consequence of the  $\pi$  symmetry of the nematic director: on a full  $2\pi$  traversal of the central point of the wave function, the streamlines of  $\Psi_{12}$  undergo a rotation by  $\pi$ , while the field itself remains continuous. The spin-nematic state is thus associated with a half-integer indexed singularity, with  $I_C = 1/2$ . Similar maps of the nematic-orbit states show dipole structures with two half-integer indexed singularities with opposite signs. These half-integer indexed topological structures are well known in optics and have been previously described in atomic systems [3].

## VI. CONCLUSION

We have demonstrated aspects of polarization in atom optics in the spin-1 regime, and showed that our Raman waveplate Hamiltonians effect an orientation-to-alignment conversion to tailor the multipole components of the atomic wave function. We examined the different forms of coupling with an external orbital angular momentum that may be achieved in such a spin-1 system. Using appropriate gauge transformations, we revealed nontrivial spin-nematic and nematic-orbit states, realized in the course of reconstructing the atomic Stokes parameters through well-known polarimetry techniques.

The density profiles of the spin components of the nematic-orbit states and the spin-nematic state were shown in Fig. 3. The relative phases between the spin components of these states were described in terms of the Stokes phase fields, and shown in Fig. 4. It is interesting to note that a measurement of the spin state populations in the circular basis can be used to reconstruct the relative phase of the quadrupolar components of the wave function, as shown with the phase field  $\Phi_{12}$ .

Our results underline the utility of recognizing the common morphological and topological characteristics of wave fields in these two different systems. We connected the atomic Stokes fields and Stokes vortices with the spin-nematic and nematic-orbit states. We were thus able to examine the topological characteristics of these atomic wave functions using the language of optics, and identify  $\pi$ - and  $2\pi$ -symmetric structures in the Stokes field streamlines. These features are characteristic of the rank-2 tensor wave field. Our results thus also highlight the significance of developing the language of atom optics to include polarization beyond the pseudo-spin-1/2 regime. The atomic multipole components for density matrices and the polarization moments for optical fields provide these connections; these results may be generalized to higher-spin systems and bichromatic optical Lissajous fields that share further higher-order symmetries [7,29].

In sum, there is much to be explored in atom-optic polarization with higher-spin systems. Atomic systems offer features, including interactions and higher-spin manifolds, which are unavailable or difficult to realize in optics. Building a common vocabulary will allow us to explore new physics in both systems.

<sup>4</sup>Note that the terminology of “vortex-antivortex pairs” is often used to describe paired vortices with opposite phase windings. Such pairs of vortices play important roles for example in the Berezinskii-Kosterlitz-Thouless transition.

### ACKNOWLEDGMENTS

We thank Elisha Haber for a careful reading of this paper. This work is supported by NSF Grant No. PHY 1708008 and by NASA Jet Propulsion Laboratory Fixed Price Contracts including Research Service Agreement (RSA) Grant No. 1656126.

### APPENDIX A: RAMAN INTERACTION

The energy eigenstates of a two-level atomic system and the right and left circular polarization states of light constitute pseudo-spin-1/2 systems. In previous work from our group, we explored polarization in atom optics in the pseudo-spin-1/2 regime. We present some of the previous results on atomic Stokes polarimetry here, for clarity.

Consider the states  $|1\rangle$  and  $|-1\rangle$  to constitute a pseudo-spin-1/2 system. We consider a two-photon Raman coupling between the states  $|1\rangle$  and  $|-1\rangle$  via an excited state  $|e\rangle$ , using optical fields with Rabi frequencies  $\Omega_A$  and  $\Omega_B$  (Fig. 2). In the limit of large detuning  $\Delta$  of the optical fields from the excited state, and for square optical pulses of duration  $t$ , the Raman interaction can be described with an analytic form after direct integration of the Schrödinger equation [4]:

$$|\psi(t)\rangle = \exp\left(i\frac{\Omega_{\text{eff}}t}{2}\right) \exp\left(i\frac{\Omega_{\text{eff}}t}{2}\vec{n}\cdot\vec{\sigma}\right)|\psi(0)\rangle \quad (\text{A1})$$

where  $\vec{n} = (\sin 2\alpha \cos \beta, \sin 2\alpha \sin \beta, \cos 2\alpha)^T$ ,  $\vec{\sigma}$  is the vector of Pauli matrices,  $\Omega_{\text{eff}} = (|\Omega_A|^2 + |\Omega_B|^2)/4\Delta$ ,  $\alpha = \arctan(|\Omega_A|/|\Omega_B|)$ , and  $\beta = \phi_A - \phi_B$  is the relative phase between the two optical Raman fields. Note that for  $|\Omega_A| = |\Omega_B| = |\Omega|$ , we defined  $\Omega_R = |\Omega|^2/4\Delta$ , and we have  $\Omega_{\text{eff}} = 2\Omega_R$ . This form of the Raman interaction is a complementary picture to the Raman Hamiltonians of Eq. (3), which highlights the effect of the Raman Hamiltonian on the atomic wave function in the pseudo-spin-1/2 regime.

### APPENDIX B: ATOMIC STOKES POLARIMETRY IN THE PSEUDO-SPIN-1/2 REGIME

The atomic Stokes parameters of the wave function  $|\psi\rangle$  [Eq. (6)] are defined in atom optics in analogy with the Stokes parameters for light. In the circular basis, the atomic Stokes parameters are

$$\begin{aligned} S_1 &= |\psi_1||\psi_{-1}| \cos \phi, \\ S_2 &= |\psi_1||\psi_{-1}| \sin \phi, \\ S_3 &= |\psi_1|^2 - |\psi_{-1}|^2, \\ S_0 &= |\psi_1|^2 + |\psi_{-1}|^2. \end{aligned} \quad (\text{B1})$$

To characterize an atomic wave function with atomic Stokes polarimetry, we need measurements of the spin state populations, and their relative phase. Our measurements are performed in the  $\hat{F}_z$  basis, and yield spin state populations. The Stokes parameters  $S_0$  and  $S_3$  are then obtained directly as the sum and difference of results from a measurement of the spin state populations of  $|\psi\rangle$ .

In order to measure  $S_1$  and  $S_2$ ,  $|\psi\rangle$  must first be transformed to change the effective measurement basis. The coherent Raman interaction can be used to realize effective ‘‘waveplates’’

for the atomic wave function [2]. Such atomic analogs of optical waveplates are realized with uniform intensity Raman fields with equal Rabi frequencies  $|\Omega_A| = |\Omega_B|$ , so that  $\vec{n} = (\cos \beta, \sin \beta, 0)$  lies in the  $S_1$ - $S_2$  plane. The pulse area  $\Omega_{\text{eff}}t$  plays the role of retardance, and the angle of the waveplate is given by  $\beta/2$ .

By using Raman waveplates with  $\beta = \pi/2$  or 0, the effective measurement basis becomes the diagonal basis of  $\hat{Q}_{x^2-y^2}$  or  $\hat{Q}_{xy}$ , respectively. The two Stokes parameters  $S_1$  and  $S_2$  may then be recovered as the differences of the populations of the wave function when measured in these transformed bases.

### APPENDIX C: EXPERIMENTAL DETAILS

In this paper our spin-1 system consists of three magnetic Zeeman sublevels  $\{|2, 2\rangle, |2, 1\rangle, |2, 0\rangle\}$  in the  $F = 2$  electronic ground state of an  $^{87}\text{Rb}$  atomic Bose-Einstein condensate, which we denote  $\{|1\rangle, |0\rangle, |-1\rangle\}$ . Our experiments are performed starting with a spin-polarized condensate of  $^{87}\text{Rb}$  with  $\approx 6.5 \times 10^6$  atoms in a magnetic trap in initial spin state  $|1\rangle \equiv |2, 2\rangle$ . The cloud is released from the trap and allowed to expand for 9 ms. A Raman pulse pair with lasers detuned 440 MHz below the  $D_1$  line of Rb and square temporal profiles couples the states  $|1\rangle \equiv |2, 2\rangle$  and  $|-1\rangle \equiv |2, 0\rangle$  via an excited state  $|e\rangle$ . A small bias magnetic field of  $\approx 11$  G breaks the degeneracy of the spin states.

To create  $|\psi\rangle$ , we use Raman beams with G and LG spatial modes. The phase difference  $\beta = \phi$  is the azimuthal phase difference between the LG and G modes. This azimuthal phase difference is transferred from the Raman beams to the atoms, with the transformation of the wave function dictated by Eq. (A1).

For the waveplate Hamiltonians, we use Raman beams with Gaussian spatial profiles with a spatial extent of about  $500 \mu\text{m}$ , so that they are relatively uniform in intensity over the size of the atomic cloud ( $50 \mu\text{m}$  in diameter at the time of the Raman interaction). The relative phase between the beams is controlled interferometrically [2], and set to be  $\beta = 0$  or  $\pi/2$  for the two quarter-waveplate operations.

### APPENDIX D: FITTING THE DATA

We use the analytic expression for the wave function after the Raman interaction to generate the theory maps in Fig. 3, which obviates the need for numerical integration of the dynamics. This wave function has the form

$$|\psi\rangle_{\text{exp}} = \sqrt{G}|1\rangle + e^{i\phi_{\text{atoms}}}\sqrt{LG}|-1\rangle, \quad (\text{D1})$$

where LG and G are the spatial modes of the Raman beams, and  $\phi_{\text{atoms}}$  denotes the relative phase between the spin states.

The mode functions that we use are

$$G \equiv \frac{\exp\left[-\frac{(x-x_0)^2}{2\sigma_x^2} - \frac{(y-y_0)^2}{2\sigma_y^2}\right]}{2\pi\sigma_x\sigma_y}, \quad (\text{D2})$$

$$\begin{aligned} \text{LG} &\equiv 4\left(\frac{(x-x_0)^2}{w_x^2} + \frac{(y-y_0)^2}{w_y^2}\right) \\ &\times \frac{\exp\left[-2\left(\frac{(x-x_0)^2}{w_x^2} + \frac{(y-y_0)^2}{w_y^2}\right)\right]}{\pi w_x w_y}. \end{aligned} \quad (\text{D3})$$

In general, the relative phase between the atomic spin states is a function of  $\beta$ , the relative phase between the Raman optical fields, but also includes extra phases conferred by the intensity-dependent ac Stark shift of the atomic energy levels, which may have a spatial variation. For Gaussian and Laguerre-Gaussian spatial modes, these phases result in an extra radial phase between the spin states. The relative phase between the spin states is thus given by [3,4]

$$\phi_{\text{atoms}} = -\arctan\left(\tan\frac{\Omega_{\text{eff}}t}{2}\cos 2\alpha\right) + \frac{\pi}{2} + \beta. \quad (\text{D4})$$

The theory maps of Fig. 3(c) are direct fits of the mode functions  $|\sqrt{G}|^2$  and  $|\sqrt{LG}|^2$  to the data. The data of Figs. 3(a) and 3(b) are obtained with a second Raman pulse pair in the quarter-waveplate configuration, this time with the relative phase between the Raman beams as  $\beta = 0$  or  $\pi/2$ . These Raman quarter waveplates create an equal superposition of the spin states, with relative phase of 0 or  $\pi/2$ . These wave

functions have the form

$$|\psi\rangle'_{\text{exp}} = \frac{1}{\sqrt{2}}[(\sqrt{G} + e^{i\phi_{\text{atoms}}}\sqrt{LG})|1\rangle + (-\sqrt{G} + e^{i\phi_{\text{atoms}}}\sqrt{LG})|-1\rangle], \quad (\text{D5})$$

and

$$|\psi\rangle''_{\text{exp}} = \frac{1}{\sqrt{2}}[(\sqrt{G} + ie^{i\phi_{\text{atoms}}}\sqrt{LG})|1\rangle + (i\sqrt{G} + e^{i\phi_{\text{atoms}}}\sqrt{LG})|-1\rangle]. \quad (\text{D6})$$

The theory maps of Figs. 3(a) and 3(b) are thus fits of the form  $|\sqrt{G} \pm \sqrt{LG}e^{i\phi_{\text{atoms}}}|^2$  and  $|\sqrt{G} \pm i\sqrt{LG}e^{i\phi_{\text{atoms}}}|^2$  to the experimental data.

The Stokes parameters are obtained as the difference in spin state populations when measured in the three bases. The experiment and theory maps of Figs. 4(a) and 4(b) are obtained from these measured and fit Stokes parameters, respectively. The ideal theory map of Fig. 4(c) is generated using the wave function of Eq. (D1), but using just the azimuthal phase  $\beta = \phi$  as the relative phase between the states.

- 
- [1] F. Schmidt-Kaler, T. Pfau, P. Schmelcher, and W. Schleich, *New J. Phys.* **12**, 065014 (2010).
- [2] J. T. Schultz, A. Hansen, and N. P. Bigelow, *Opt. Lett.* **39**, 4271 (2014).
- [3] A. Hansen, J. T. Schultz, and N. P. Bigelow, *Optica* **3**, 355 (2016).
- [4] J. T. Schultz, A. Hansen, J. D. Murphree, M. Jayaseelan, and N. P. Bigelow, *J. Opt.* **18**, 064009 (2016).
- [5] V. Kumar and N. K. Viswanathan, *J. Opt. Soc. Am. B* **31**, A40 (2014).
- [6] K. E. Ballantine, J. F. Donegan, and P. R. Eastham, *Sci. Adv.* **2**, e1501748 (2016).
- [7] E. Pisanty, G. J. Machado, V. Vicuña-Hernández, A. Picón, A. Celi, J. P. Torres, and M. Lewenstein, *Nat. Photonics* **13**, 569 (2019).
- [8] T. Bauer, P. Banzer, E. Karimi, S. Orlov, A. Rubano, L. Marrucci, E. Santamato, R. W. Boyd, and G. Leuchs, *Science* **347**, 964 (2015).
- [9] Y. J. Lin, K. Jiménez-García, and I. B. Spielman, *Nature (London)* **471**, 83 (2011).
- [10] P. Wang, Z.-Q. Yu, Z. Fu, J. Miao, L. Huang, S. Chai, H. Zhai, and J. Zhang, *Phys. Rev. Lett.* **109**, 095301 (2012).
- [11] L. W. Cheuk, A. T. Sommer, Z. Hadzibabic, T. Yefsah, W. S. Bakr, and M. W. Zwierlein, *Phys. Rev. Lett.* **109**, 095302 (2012).
- [12] H.-R. Chen, K.-Y. Lin, P.-K. Chen, N.-C. Chiu, J.-B. Wang, C.-A. Chen, P. Huang, S.-K. Yip, Y. Kawaguchi, and Y.-J. Lin, *Phys. Rev. Lett.* **121**, 113204 (2018).
- [13] D. Zhang, T. Gao, P. Zou, L. Kong, R. Li, X. Shen, X.-L. Chen, S.-G. Peng, M. Zhan, H. Pu, and K. Jiang, *Phys. Rev. Lett.* **122**, 110402 (2019).
- [14] X.-W. Luo, K. Sun, and C. Zhang, *Phys. Rev. Lett.* **119**, 193001 (2017).
- [15] L. Chen, Y. Zhang, and H. Pu, *Phys. Rev. Lett.* **125**, 195303 (2020).
- [16] D. Lao, C. Raman, and C. A. R. Sá de Melo, *Phys. Rev. Lett.* **124**, 173203 (2020).
- [17] X. Qiu, A.-Y. Hu, Y. Cai, H. Saito, X.-F. Zhang, and L. Wen, *Phys. Rev. A* **107**, 033308 (2023).
- [18] E. Wolf, *Nuovo Cim* **12**, 884 (1954).
- [19] C. Brosseau, *Fundamentals of Polarized Light: A Statistical Optics Approach* (Wiley, 1998).
- [20] Y. Kawaguchi and M. Ueda, *Phys. Rep.* **520**, 253 (2012).
- [21] J. J. Sakurai and J. Napolitano, *Modern Quantum Mechanics*, 2nd ed. (Addison-Wesley, Reading, MA, 2011).
- [22] M. Kitagawa and M. Ueda, *Phys. Rev. A* **47**, 5138 (1993).
- [23] I. Freund, *Opt. Lett.* **26**, 1996 (2001).
- [24] I. Freund, *Opt. Commun.* **201**, 251 (2002).
- [25] I. Freund, A. I. Mokhun, M. S. Soskin, O. V. Angelsky, and I. I. Mokhun, *Opt. Lett.* **27**, 545 (2002).
- [26] G. Gbur, *Singular Optics* (CRC, Boca Raton, FL, 2015), pp. 1–23.
- [27] G. Arora, S. Deepa, S. N. Khan, and P. Senthikumar, *Sci. Rep.* **10**, 20759 (2020).
- [28] M. R. Dennis, *Opt. Commun.* **213**, 201 (2002).
- [29] I. Freund, *Opt. Commun.* **226**, 351 (2003).